Clim Dyn (2014) 42:1487–1508
DOI 10.1007/s00382-013-1831-8

Subseasonal forecast skills and biases of global summer monsoons in the NCEP Climate Forecast System version 2

Xiangwen Liu · Song Yang · Qiaoping Li · Arun Kumar · Scott Weaver · Shi Liu

Received: 2 November 2012 / Accepted: 4 June 2013 / Published online: 15 June 2013

Abstract Subseasonal forecast skills and biases of global summer monsoons are diagnosed using daily data from the hindcasts of 45-day integrations by the NCEP Climate Forecast System version 2. Predictions for subseasonal variability of zonal wind and precipitation are generally more skillful over the Asian and Australian monsoon regions than other monsoon regions. Climatologically, forecasts for the variations of dynamical monsoon indices have high skills at leads of about 2 weeks. However, apparent interannual differences exist, with high skills up to 5 weeks in exceptional cases. Comparisons for the relationships of monsoon indices with atmospheric circulation and precipitation patterns between skillful and unskillful forecasts indicate that skills for subseasonal variability of a monsoon index depend partially on the degree to which the observed variability of the index attributes to the variation of large-scale circulation. Thus, predictions are often more skillful when the index is closely linked to atmospheric circulation over a broad region than over a regional and narrow range. It is also revealed that, the subseasonal variations of biases of winds, precipitation, and surface temperature over various monsoon regions are captured by a first mode with seasonally independent biases and a second mode with apparent phase transition of biases during summer. The first mode indicates the dominance of overall weaker-than-observed summer monsoons over major monsoon regions. However, at certain stages of monsoon evolution, these underestimations are regionally offset or intensified by the time evolving biases portrayed by the second mode. This feature may be partially related to factors such as the shifts of subtropical highs and intertropical convergence zones, the reversal of biases of surface temperature over some monsoon regions, and the transition of regional circulation system. The significant geographical differences in bias growth with increasing lead time reflect the distinctions of initial memory capability of the climate system over different monsoon regions.

Keywords Global monsoons · Subseasonal prediction biases · Subseasonal prediction skill · NCEP CFSv2

X. Liu · Q. Li
National Climate Center, China Meteorological Administration, Beijing, China

S. Yang (✉)
Department of Atmospheric Sciences, Sun Yat-sen University, 135 West Xingang Road, Guangzhou 510275, Guangdong, China
e-mail: yangsong3@mail.sysu.edu.cn

A. Kumar · S. Weaver
NOAA Climate Prediction Center, College Park, MD, USA

S. Liu
Institute of Meteorological Sciences of Jilin Province, Changchun, Jilin, China

1 Introduction

Monsoon as a key element of the global climate system is closely related to many prominent weather and climate phenomena. It strongly affects human activities and economic wellbeing of the world. Due to its complex variability and enormous social and economic impacts, monsoon prediction has long been an important but challenging task.

In the past decades, dynamical prediction has advanced significantly and become an indispensable approach in monsoon research and forecast operations. Based on the

hypothesis that seasonal atmospheric predictability originates from the boundary forcing at the earth's surface (Charney and Shukla 1981), predictions with two-tier approach, which are made by atmosphere-alone models forced by prescribed sea surface temperature, provide reasonable skills to a certain extent (Kang et al. 2002; Moron et al. 2004; Zhou et al. 2009; Xue et al. 2010). Nevertheless, two-tier predictions for monsoons, especially the Asian-Australian monsoon, show apparent deficiencies due to unrealistic air-sea interaction (Wang et al. 2004, 2005; Kumar et al. 2005; Misra 2008). On the other hand, monsoon prediction with coupled atmosphere–ocean-land models is more promising and has potential for improvements with enhancement of model resolutions and initial conditions (Pope and Stratton 2002; Yang et al. 2009; Wen et al. 2012), improvement of model physics (Yhang and Hong 2008; Yang et al. 2011), and application of multi-model ensemble methods (Krishnamurti et al. 2006; Wang et al. 2008), among others.

However, monsoon prediction with coupled models suffers from apparent biases, which affect accurate simulation and forecast of monsoon variability and its relationship with other climate systems (e.g., Chen et al. 2000; Turner et al. 2005; Lee et al. 2010). Also, climate models tend to underestimate the variance of monsoon variability although they are able to reproduce the dominant modes (Wang et al. 2008; Xue et al. 2010). They can predict large-scale monsoon features related to strong oceanic-atmospheric events such as El Niño–Southern Oscillation (ENSO) and the Indian Ocean Dipole, in contrast to the unskillful performance in simulating more regional characteristics (Yang et al. 2008a; Drbohlav and Krishnamurthy 2010). Predictions are also not skillful for limited representation of subseasonal variability (Higgins et al. 2008; Yang et al. 2008b; Fu et al. 2009; Pegion and Sardeshmukh 2011). For a comprehensive understanding of the above limitations and improvement of monsoon prediction accuracy, assessing the skills and diagnosing biases of dynamical monsoon prediction have become an important subject in both academic and operational communities.

The National Centers for Environmental Prediction (NCEP) implemented the first version (Saha et al. 2006) and the second version of Climate Forecast System (CFS) to provide operational monthly-seasonal predictions in August 2004 and March 2011, respectively. Based on comprehensive retrospective forecasts, previous studies have demonstrated that the CFS is able to capture the variations of the Asian monsoon (e.g., Yang et al. 2008a; Liang et al. 2009; Drbohlav and Krishnamurthy 2010; Li and Yang 2010; Lee et al. 2011), the South American summer monsoon (e.g., Misra and Zhang 2007; Jones et al. 2012), the North American summer monsoon (e.g., Higgins et al. 2008; Yang et al. 2009), the West African summer monsoon (e.g., Xue et al. 2010), among others. These studies have shown encouraging results, although monsoon predictability, especially on subseasonal time scale, has not been fully addressed. Moreover, improvement of forecast skills in monthly and intraseasonal climate variability due to upgrade of models (e.g., Yuan et al. 2011; Weaver et al. 2011) may promise a better prospect for monsoon prediction.

Therefore, in this study, we explore the forecast skills of subseasonal variability of global summer monsoons in the NCEP CFS (CFSv2), including the South Asian monsoon (SAM), the Southeast Asian monsoon (SEAM), the West African monsoon (WAFM), the North American monsoon (NAMM), the South American monsoon (SAMM), and the Australian monsoon (AUM). The following questions are addressed: What are the subseasonal forecast skills of global summer monsoons in the CFSv2? How do subseasonal prediction skills change on interannual scale? How different are the biases during the different stages of monsoon evolution and as a function of lead time? What are the atmospheric and oceanic processes related to these differences?

In Sect. 2, a brief overview of the model output and data analyzed is provided. In Sects. 3–5, we analyze the multi-year mean features of first-month forecasts, subseasonal prediction skill of summer monsoons, and subseasonal variations of biases with lead time, respectively. Summary and discussions are given in Sect. 6. It should be noted that, the bias diagnostics in Sect. 5 is presented after the analyses of prediction skill in Sect. 4 because Sects. 3 and 4 provide analyses from a global point of view while Sect. 5 only concerns regional features. In addition, the former provides a foundation on the choices of monsoon regions and lead time and the understanding of some features discussed in the later section.

2 Model output and observational data

The CFSv2 is a coupled atmosphere–ocean-land-sea ice dynamical seasonal prediction system. The atmospheric component is the NCEP Atmospheric Global Forecast System with a T126 horizontal resolution and 64 sigma layers in the vertical. The oceanic component is the Geophysical Fluid Dynamics Laboratory Modular Ocean Model version 4 coupled with a two-layer sea ice model, and the land model is the NCEP, OSU, Air Force, and Hydrologic Research Laboratory model. The different components are coupled without any flux correction. The initial conditions are obtained from the Climate Forecast System Reanalysis (CFSR; Saha et al. 2010).

The retrospective forecasts from the CFSv2 are utilized in this study. They are 45-day integrations initiated from

every 0, 6, 12, and 18 UTC cycle from 1999 to 2010. The observations used for model verification include atmospheric variables and surface temperature from the CFSR and the global CMORPH precipitation data from Climate Prediction Center (Joyce et al. 2004). In this work, the CFSR and CMORPH with high temporal and spatial resolutions are all interpolated to daily-average data with a same horizontal resolution with CFSv2.

In our study, for a specific predicted target month (or pentad), lead 0 is defined as the forecasts initialized on the first day of the month (or pentad), lead 1 denotes the forecasts initialized on the last day of the previous month (or pentad), lead 2 for the model runs initialized 2 days ahead to the last day of the target, and so on. Each prediction of a lead is an ensemble mean of four members.

3 Model drift in first forecast month

To explore the model drift in first forecast month, ensemble means of predictions with leads of 0–5 days for the next target months in boreal summer (May–September) and austral summer (November–March) during 1999–2010 are examined. Although the CFSv2 captures the major features of northern and southern summer monsoons, apparent biases are found over various monsoon regions. Figures 1 and 2 show the predicted 12-year means for precipitation and 850-hPa winds and their biases averaged over boreal summer and austral summer, respectively.

For the Asian summer monsoon, a cyclonic wind bias dominates over the northwestern Pacific, associated with a dry bias over the western edge of WPSH and a wet bias associated with the cyclonic wind bias. Easterly wind bias occurs over South Asia and westerly wind bias appears over the equatorial Indian Ocean, along with extraordinarily lack of precipitation over India and the Bay of Bengal and overestimated precipitation over the eastern Arabian Sea and the central-eastern equatorial Indian Ocean. Besides, weaker-than-observed meridional wind and precipitation are seen over the South China Sea. In contrast to the dry biases over the Bay of Bengal and the South China Sea, wet biases appear over the southern flank of the Tibetan Plateau and the west coast of the Indo-China Peninsula in the CFSv2, a problem in the CFS version 1 (Yang et al. 2008a; Drbohlav and Krishnamurthy 2010) and some multi-model ensembles of the DEMETER and ENSEMBLES EU projects (Lee et al. 2010; Li et al. 2012; Rajeevan et al. 2012) as well. These features suggest some common deficiencies in current climate models. Over the African summer monsoon region, an underestimation of precipitation, as a response to a westerly wind bias over the equatorial area and a cyclonic wind bias over the Sahara Desert, indicating a weaker ITCZ, appears over most of West Africa. Also, apparent northwesterly wind bias and dry bias over southwestern North America exist in boreal summer, meaning that the predicted NAMM is often weaker than observed.

For the southern summer monsoons (Fig. 2), the predicted AUM is often featured by a conspicuous southerly wind bias over northern Australia and a stronger-than-observed wind convergence near the equator, as well as a dry bias over northern Australia and a wet bias over the equatorial area owing to the farther north position of model ITCZ than observed. Except over the Andes Mountains and the northern edge of the Amazon Basin, most of South America is dominated by an apparent dry bias in austral summer, along with southerly wind bias to the north of Amazon and anticyclonic wind bias over eastern Brazil.

We further plot the differences in 12-year mean surface temperature between the model and observations (Fig. 3). During boreal summer (Fig. 3a), conspicuous warm biases extend from the Sahara Desert to most of the Tibetan Plateau, with amplitude of more than 2 °C in many places. Conversely, to the south of the warm biases, equally apparent cold biases are found from West Africa to the Ethiopian Highland. Over the Asian monsoon region, as a possible response to the dry bias over the western edge of WPSH and the cyclonic wind bias over the northwestern Pacific, the warmer water in the tropical western Pacific and the colder water in the subtropical North Pacific exist in summer. Also, the warmer water over the South China Sea and the colder land over the Indo-China Peninsula and South China persist in summer, and opposite-sign biases are found to the north and the south of the Indian Peninsula. In addition, apparent cold biases appear over most of North America except near the Gulf of California and over the Rocky Mountains, while warm biases often occur over the northeastern Pacific and the Gulf of Mexico.

During austral summer (Fig. 3b), most of South America, except the northwestern Amazon Basin, is often dominated by apparent cold biases, while the adjacent southeastern Pacific is occupied by warm biases. Over the AUM region, warm biases persist over most tropical areas except the Maritime Continent.

4 Subseasonal prediction skills

In this section, we discuss the subseasonal prediction of monsoons as a function of lead time, focusing on the prediction skills in winds, precipitation, and monsoon indices. The subseasonal variations in boreal summer and austral summer are examined for pentad means, i.e., Julian pentads 25–54 from May to September and pentads 61–72 and 1–18 from November to March, respectively. The predictions for a target pentad are divided into 14 groups

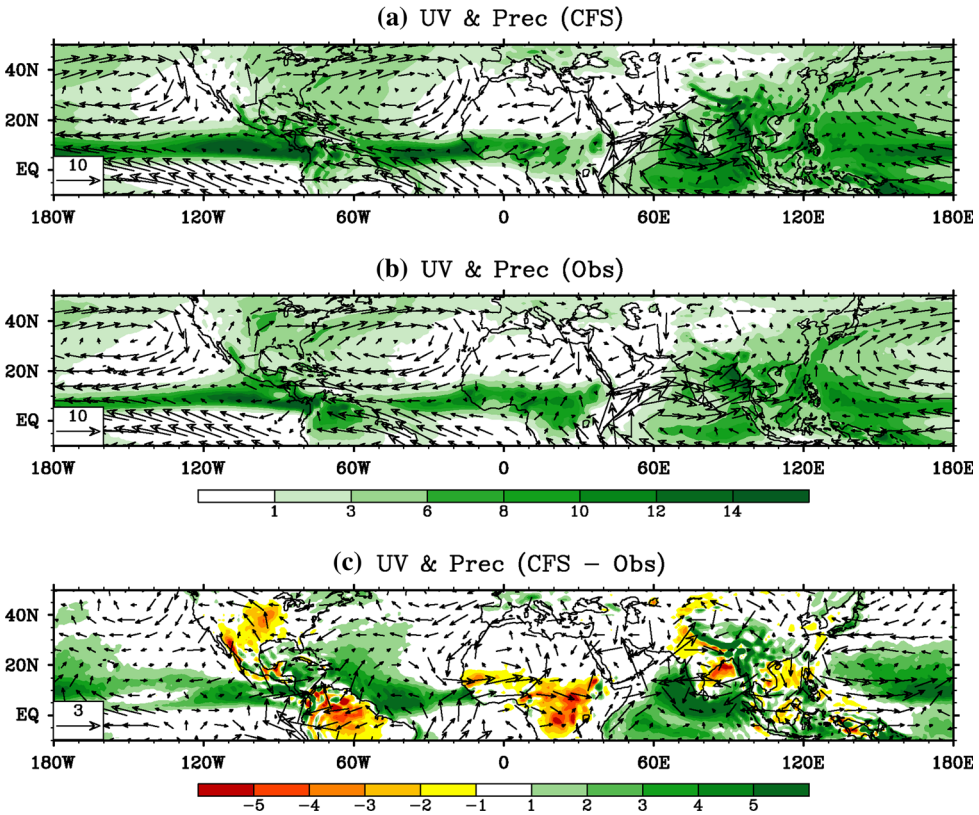

Fig. 1 Twelve-year means of precipitation (*shadings*, units mm/day) and 850-hPa winds (*vectors*, units m/s) for **a** first-month forecasts, **b** observations, and **c** biases (predictions minus observations) averaged from May to September

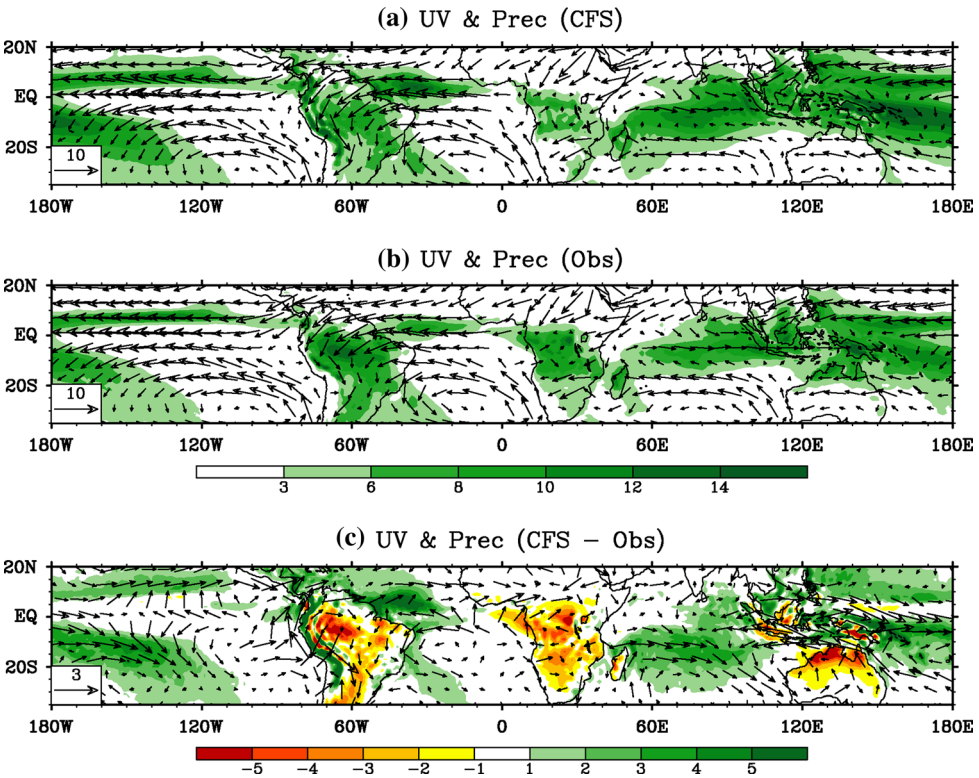

Fig. 2 Same as Fig. 1 but for features averaged from November to March

according to the length of lead time, i.e. 0–2, 3–5, and every 3 days to 39–40 days. Most of these pentad predictions are ensemble means of 12 members within 3 days, except that the last prediction is an ensemble average of 8 members within 2 days. For different leads of time, and for each pentad in a certain year, the pentad-mean anomalies

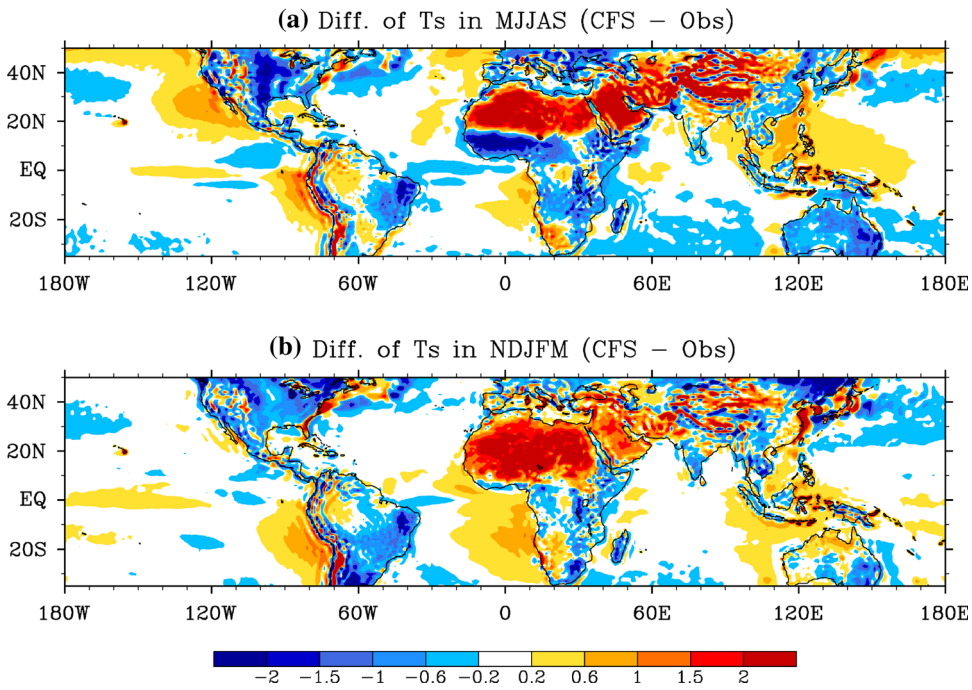

Fig. 3 Differences between first-month forecasts and observations for 12-year mean surface temperatures (units °C) averaged from **a** May to September and **b** November to March

are computed by subtracting the corresponding pentad climatologies from 1999 to 2010.

4.1 Standard deviations and forecast errors of winds and precipitation

The top two panels of Fig. 4 show the observed and predicted standard deviations of pentad variations of 850-hPa zonal wind and precipitation in boreal summer. The predictions with the shortest leads (0–2 days) agree well with observations in many major centers, especially over the northern Pacific, the northern Atlantic, and southern Asia with large zonal wind variability, and over the eastern tropical Pacific, the eastern equatorial Atlantic, and Asian tropical oceans with large precipitation variability. However, the magnitude of predicted variability is often weaker than observed, which may be partially due to underestimation by the model or smoothing by the ensemble averaging process. With increasing lead time, the standard deviations of zonal wind and rainfall show clearly a decreasing tendency owing to the gradual domination of forecast signals from slowly varying components of the climate system (figure not shown).

The root-mean-square errors (RMSE) of predicted zonal wind and precipitation are further depicted by the other panels of Fig. 4. Distribution features similar to the above-discussed standard deviation features are found for most predictions, indicating the concurrence of significant error growth and strong climate variability, whereas the errors show apparent variation with lead time. The errors of zonal wind exhibit a very small magnitude at the shortest leads (figure not shown), followed by a gradual increase to a persistent state with the advance of lead time as shown in Figs. 4c–f. Error growth is mainly concentrated in the leads up to 2 weeks for zonal wind in most areas, except over southern Asia. In contrast with zonal wind, the errors of precipitation (Fig. 4i–l) show more rapid development, resulting in large amplitude at the minimum lead time, and major growth is almost confined to the leads up to 1 week. This feature implies that precipitation bias rapidly evolves towards its asymptotic value and precipitation attains its upper limit of actual predictability in the model, although the atmospheric circulation still has growing errors and is with considerable skills at that time. Besides, it should be noted that the precipitation over some regions, especially the subtropical Asian continent and the areas from tropical eastern Pacific to tropical West Africa, suffers from an initial shock featured by a large error at the shortest leads with a subsequent reduction.

The features of standard deviations and forecast errors in austral summer are presented in Fig. 5. The large errors, associated with strong subseasonal variability, are mainly distributed around the ITCZ, South America, the South Pacific, and the South Indian Ocean. Likewise, the error growth is mainly concentrated for leads <2 weeks for zonal wind as compared to 1 week for precipitation. To some extent, the enduring slower increase in RMSE of zonal wind to the north of Australia implies a larger predictability of the AUM low-level circulation in the model.

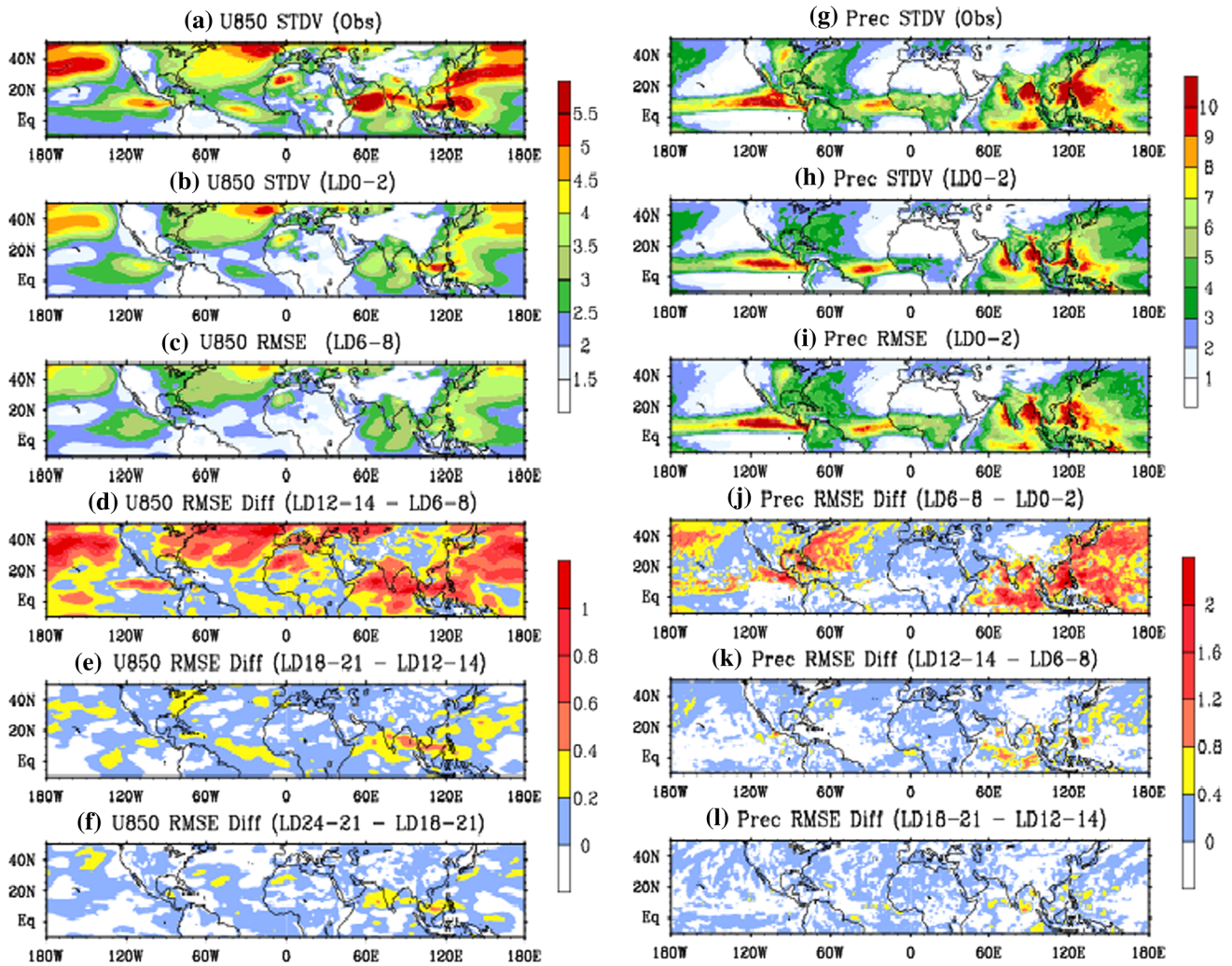

Fig. 4 *Left panels* for 850-mb zonal wind (units ms^{-1}): **a** observed standard deviation, **b** CFSv2 standard deviation, **c** CFSv2 RMSE for leads of 6–8 days, and **d**–**f** differences in CFSv2 RMSE between different leads. *Right panels* are similarly shown for precipitation (units mm/day). Values are the 12-year means for boreal summer (May–September) from 1999 to 2010 and the mean seasonal cycle is removed for each year

4.2 Forecast skills of monsoon indices

For the observed and predicted time sequences of pentad anomalies (30 pentads in boreal or austral summer) in each year, temporal correlations between observations and predictions of different leads are calculated to evaluate the skills in forecasting the temporal variability of winds and precipitation over the entire monsoon season. Multi-year mean skill for 850-hPa zonal wind in boreal summer and austral summer are shown in Fig. 6. The model skillfully captures the subseasonal variation of zonal wind over most areas for 1-week lead forecasts. It exhibits a rapid and remarkable loss of skill as lead time increases to about 2 weeks, although significant skills can still be found over some equatorial areas, including the southern South China Sea, the equatorial Atlantic, and the western Indian Ocean in boreal summer, as well as most equatorial regions except the eastern Pacific in austral summer. At the leads of about 3 weeks, the predictions of zonal wind are unskillful over most areas, except some sparse regions near the equator in the Asian and Australian monsoon regions. In comparison, the skills of precipitation prediction show a much more rapid decrease with lead time over most areas, and they often drop to insignificant level at the leads of about 1 week (figure not shown).

Although the predictions of grid-point precipitation are disappointing, area-averaged rainfall is more predictable. Here, we discuss the skills of prediction of regional averaged precipitation for SAM, SEAM, WAFM, NAMM, SAMM, and AUM. The selected regions basically cover the places with concentrated monsoon rainfall and maximum precipitation variability. The domains of these regions are listed in Table 1 (also outlined in Fig. 6), and the same regions have been used in previous studies (e.g., Lau et al.

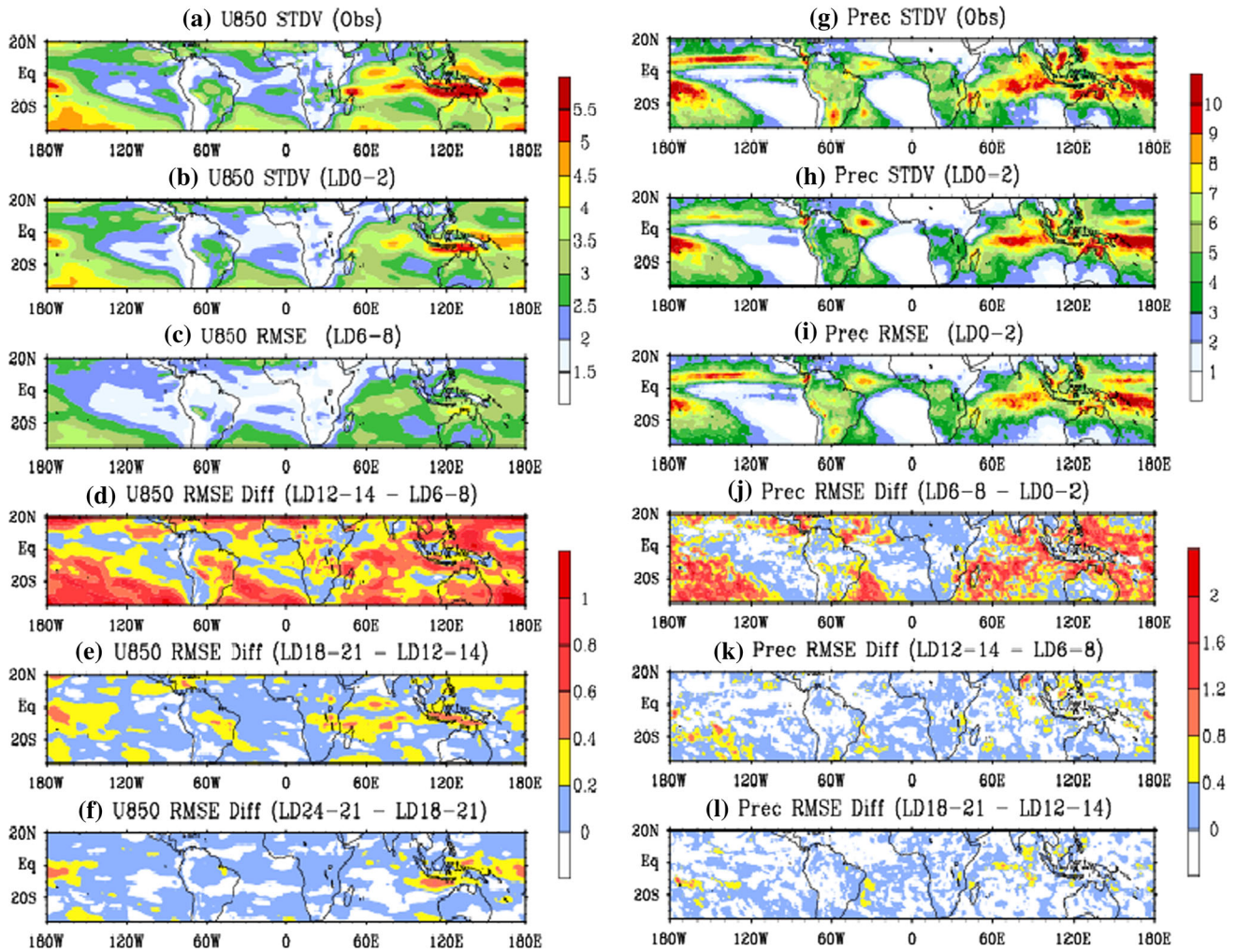

Fig. 5 Same as Fig. 4 but for climatological means for austral summer (November–March) from 1999 to 2009

2000; Xue et al. 2010; Vera et al. 2006; Kajikawa et al. 2009) to investigate the variability of monsoon precipitation. Figure 7a shows the correlations between observations and forecasts as a function of lead time for precipitation for different years. The forecast skills for all regions show conspicuous interannual differences. For example, the forecasts for AUM in 2001 and SAMM in 2003 are skillful at leads up to 5 weeks, while the AUM in 2008 and the SAMM in 2004 only show skills within 1-week leads. On average, the skill drops below the 99 % confidence level in about 2 weeks for WAFM and SAMM, one and a half weeks for SAM, SEAM and AUM, and <1 week for NAMM. The low skill for NAMM may be partially attributed to model's inability in capturing the regional precipitation with weak variability and small spatial scale.

We further investigate the prediction skills of monsoon indices (Fig. 7b) including the Webster-Yang index (WYI; Webster and Yang 1992), the SAM index (Goswami et al. 1999), the SEAM index (Wang and Fan 1999), the AUM index (Kajikawa et al. 2009), and a zonal wind shear index (ZWSI) and a meridional wind shear index (MWSI) for the SAMM (Gan et al. 2005). The definitions of these indices are given in Table 1. On average, it takes about 2 weeks of leads for WYI, SAM index, SAMM-ZWSI and SAMM-MWSI, and about two and a half weeks of leads for SEAM index and AUM index to fall into the range of unskillful predictions. However, the prediction of each index shows apparent interannual differences, with high skills at the leads up to 5 weeks in some years but <2 weeks in other years. Specially, the Asian and Australian monsoon indices show larger spreads of skill than the South American monsoon indices. Forecast skill generally shows an apparent decreasing tendency with increasing lead time at short leads, especially those <2 weeks, followed by continuous and rapid descent (e.g., WYI in 2003, SAM in 2010, SEAM in 2005, and AUM in 2008), or a persistency with rarely-varying magnitude (e.g., WYI in 2005 and SAM in 2002), or a gradual increase again at long leads (e.g., SEAM in 2008 and AUM in 2001). The persistently

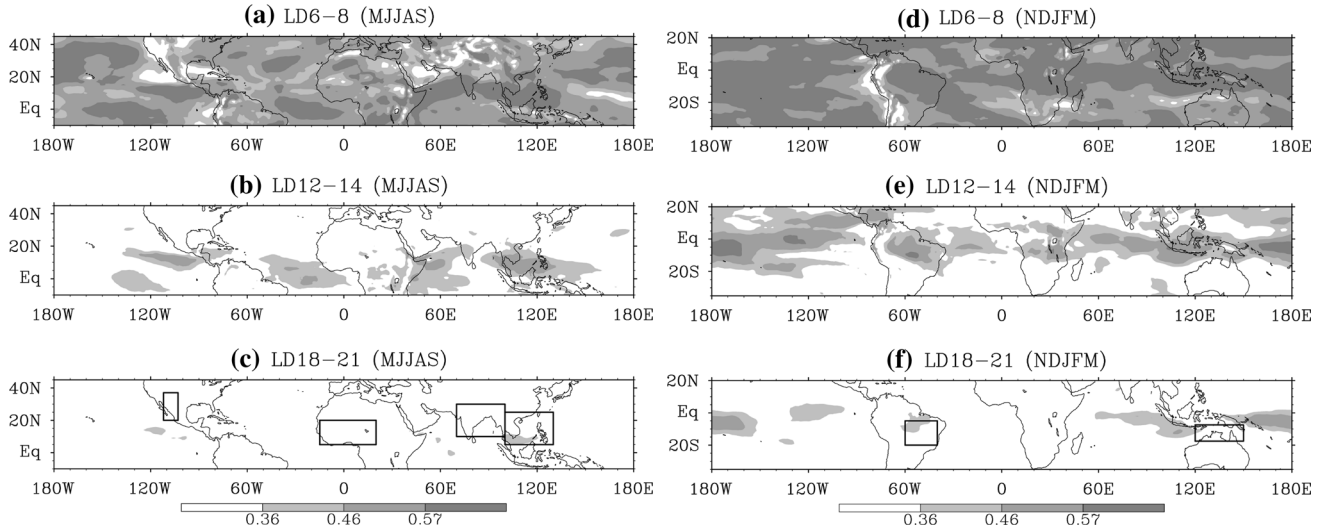

Fig. 6 Spatial distributions of temporal correlation between observations and predictions of different leads for 850-hPa zonal wind from May to September (*left column*) and from November to March (*right column*). Shown are the 12-year averages for boreal summer from 1999 to 2010 and 11-year averages for austral summer from 1999 to 2009. The mean seasonal cycle is removed for each year. The three *shading* levels represent the statistical significance of correlation above the 95, 99, and 99.9 % confidence levels, respectively. *Black rectangles* indicate different monsoon regions

Table 1 List of monsoon indices defined by precipitation and atmospheric circulation

Type	Index abbreviation	Definition (variables and the domain range to average)
Regional averaged precipitation	SAM	Prec (10°–30°N, 70°–100°E)
	SEAM	Prec (5°–25°N, 100°–130°E)
	WAFM	Prec (5°–20°N, 15°W–20°E)
	NAMM	Prec (20°–37°N, 103°–112°W)
	AUM	Prec (7.5°–17.5°S, 120°–150°E)
	SAMM	Prec (5°–20°S, 40°–60°W)
Dynamical monsoon indices	WY	U_{850}–U_{200} (0°–20°N, 40°–110°E)
	SAM	V_{850}–V_{200} (10°–30°N, 70°–110°E)
	SEAM	U_{850} (5°–15°N, 90°–130°E)–U_{850} (22.5°–32.5°N, 110°–140°E)
	AUM	U_{850} (5°–15°S, 110°–130°E)
	SAMM-ZWSI	U_{850}–U_{200} (10°–15°S, 50°–60°W)
	SAMM-MWSI	V_{850}–V_{200} (5°–10°S, 30°–40°W)

significant skills for subseasonal predictions may be more attributable to the signals from slowly varying components of the climate system, since the initial memories of rapidly varying parts wither quickly with advancing leads.

Besides, the summer-averaged spatial correlation between observations and forecasts as a function of lead time for the precipitation and 850-hPa zonal wind in various monsoon regions is presented in Fig. 8. On the whole, significantly higher skills are found for zonal wind than for precipitation, and for the Asian monsoon (especially the SEAM) than for other monsoons. There exist different but considerably smaller interannual differences for spatial correlation skills as compared to temporal correlation skills of monsoon forecasts.

4.3 Prediction of relationships between monsoon indices and circulation

The relationships between monsoon indices and atmospheric circulation patterns are further evaluated in this section, with a focus on the skillful and unskillful cases shown in Sect. 4.2. The observations and predictions of different leads for WYI, SEAM, AUM, SAMM-ZWSI, NAMM, and WAFM indices in the years of most and least significant skills are shown in Figs. 9, 10 and 11. The features for other monsoon indices and secondary skillful cases are also analyzed but figures are not shown.

In 2005, the observed WYI is an excellent measure of the variability of low-level winds over the east coast of Africa, the Arabian Sea, India, and the Bay of Bengal. A stronger-than-normal WYI is associated with more vigorous cross-equatorial flow (CEF) near Somali and zonal wind over South Asia. This link is similar to the response of atmospheric circulation to the enhanced convection over the Bay of Bengal on interannual time scale (Wang and Fan 1999). The CFSv2 is able to capture the observed correlation reasonably well at all leads. Nevertheless, it gradually overestimates the relationship in both intensity and spatial extension and partially reflects an increasing response to the convection near the Philippines with advance of lead time.

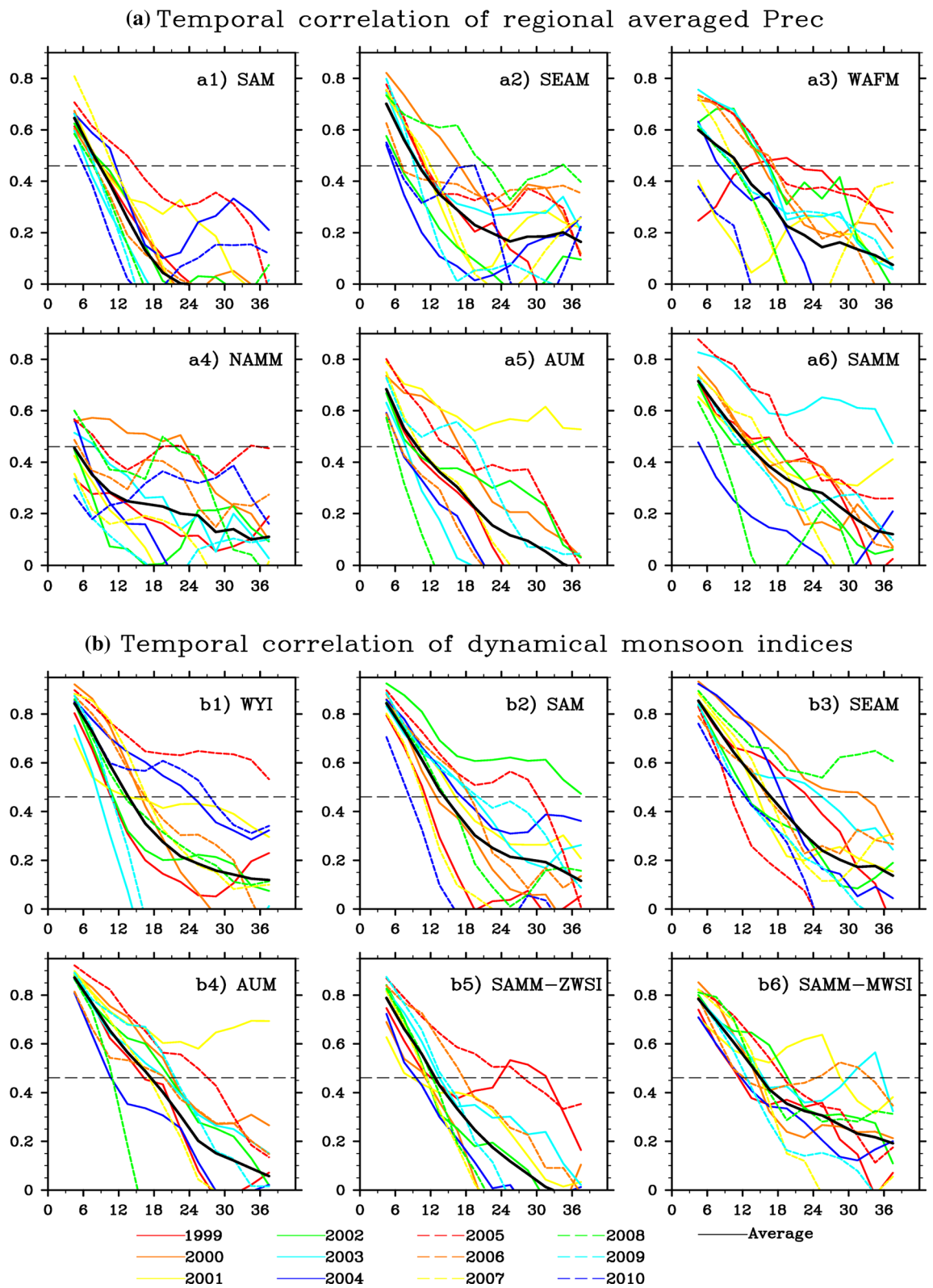

Fig. 7 Temporal correlations between observations and forecasts of different lead days (*horizontal axis*) for **a** regionally averaged precipitation and **b** dynamical monsoon indices listed in Table 1. Shown are the three-point running averages along forecast lead days. *Black dash lines* denote the statistical significance of correlation at the 99 % confidence level

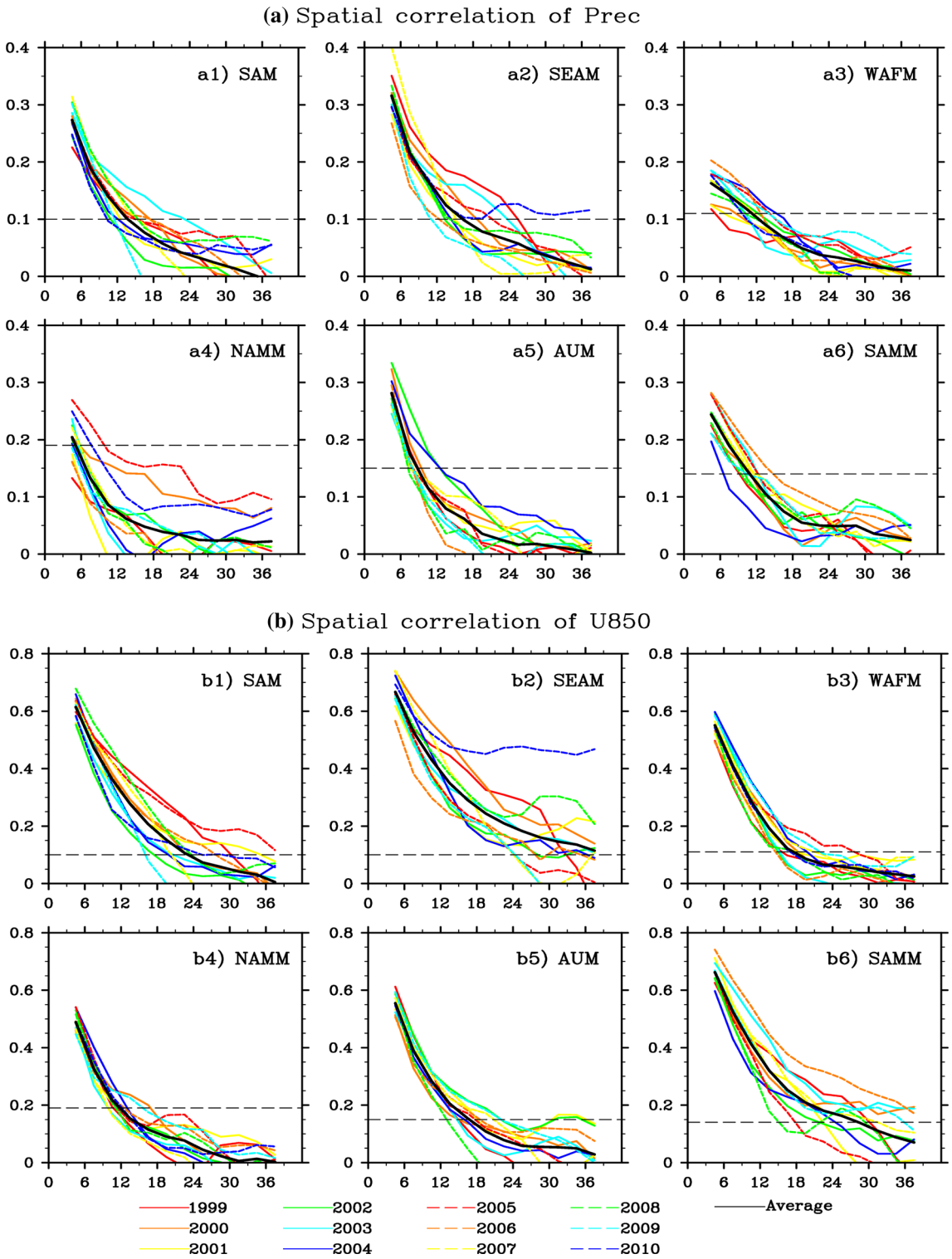

Fig. 8 Summer-averaged spatial correlations between observations and forecasts of different lead days (*horizontal axis*) for **a** precipitation and **b** 850-hPa zonal wind in monsoon regions outlined in Fig. 6. Shown are the three-point running averages along forecast lead days. *Black dash lines* denote the statistical significance of correlation at the 99 % confidence level

In contrast, the observed WYI in 2003 is strongly correlated with the zonal wind over the equatorial Indian Ocean, but this relationship is rapidly replaced by a strengthening link between WYI and the zonal wind over southern Asia with increasing leads as a large-scale response to the convections over the Bay of Bengal and

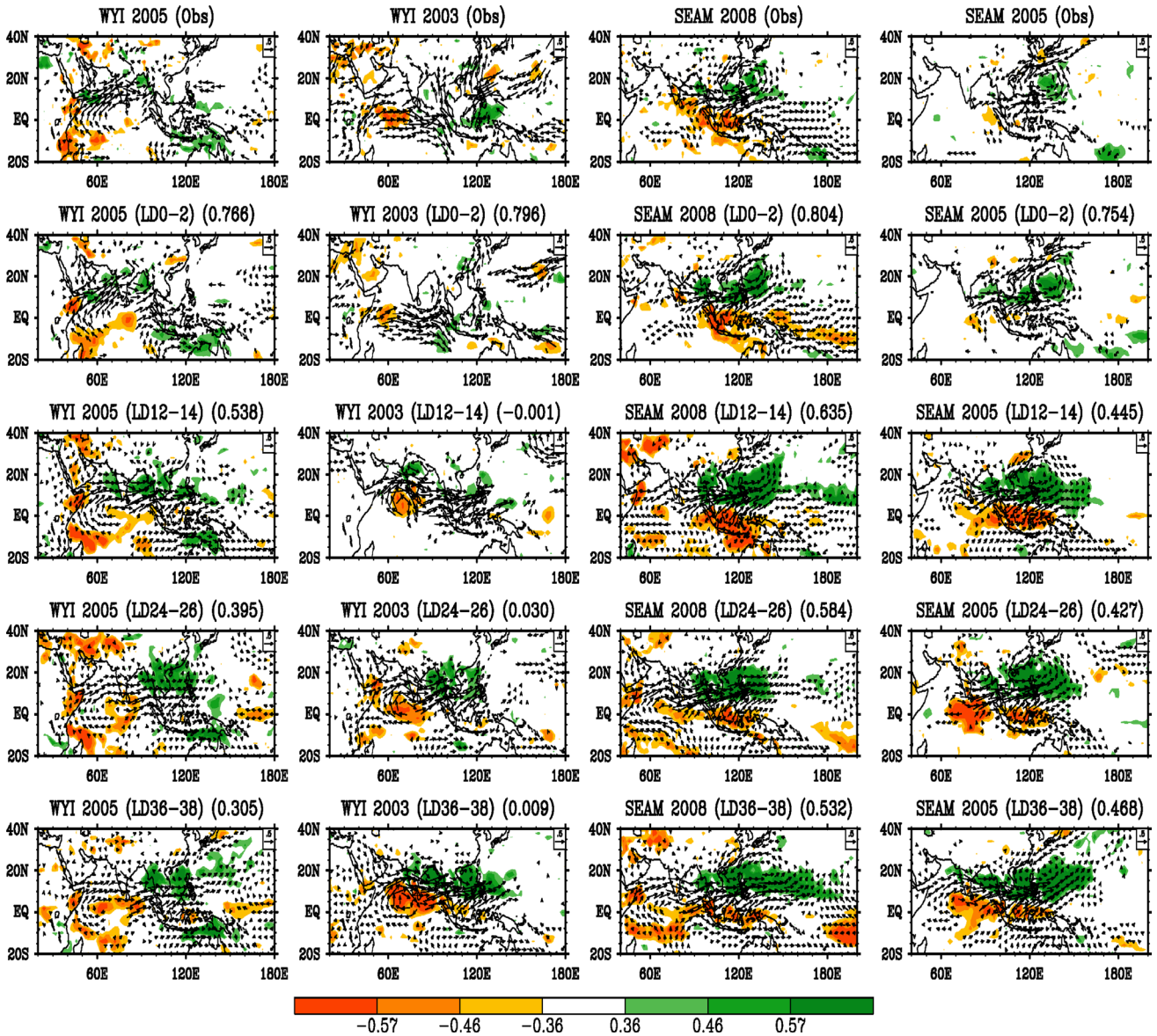

Fig. 9 Patterns of correlations (*shadings*) between precipitation and monsoon indices and regressions (*vectors*) of 850-hPa winds on monsoon indices. Features are presented for observations and for predictions of different leads. Shown are for Webster-Yang index (*left two columns*) and Southeast Asian monsoon index (*right two columns*) in higher-skill years (*first and third columns*) and lower-skill years (*second and fourth columns*). The three *shading* levels represent the statistical significance of correlation above the 95, 99, and 99.9 % confidence levels respectively, and the *decimals* shown in the right of headlines are spatial pattern correlations between predicted and observed features

near the Philippines. This result means an unskillful prediction of WYI in 2003.

For the SEAM index, the predictions in both 2008 and 2005 tend to indicate a gradually intensifying large-scale response to the convection over the western tropical Pacific with increasing lead time. The overall features are that a stronger SEAM corresponds to more robust cyclonic convergence anomalies over Southeast Asia and westerly wind anomalies from the Indian Peninsula to the Philippines, and corresponds to more precipitation over the western tropical Pacific and less precipitation over the Maritime Continent. However, the former is more skillful than the latter, because the observed variability of SEAM is attributed more to the variation of large-scale circulation and convection anomaly in 2008 compared to 2005.

The observation in 2001 shows that, a higher-than-normal AUM index not only corresponds to stronger westerly wind across southern Indonesia and northern Australia associated with more precipitation off the north coast of Australia, but also couples with cyclonic anomaly over northwestern Australia. The CFSv2 is able to skillfully reproduce the observed relationship at short leads.

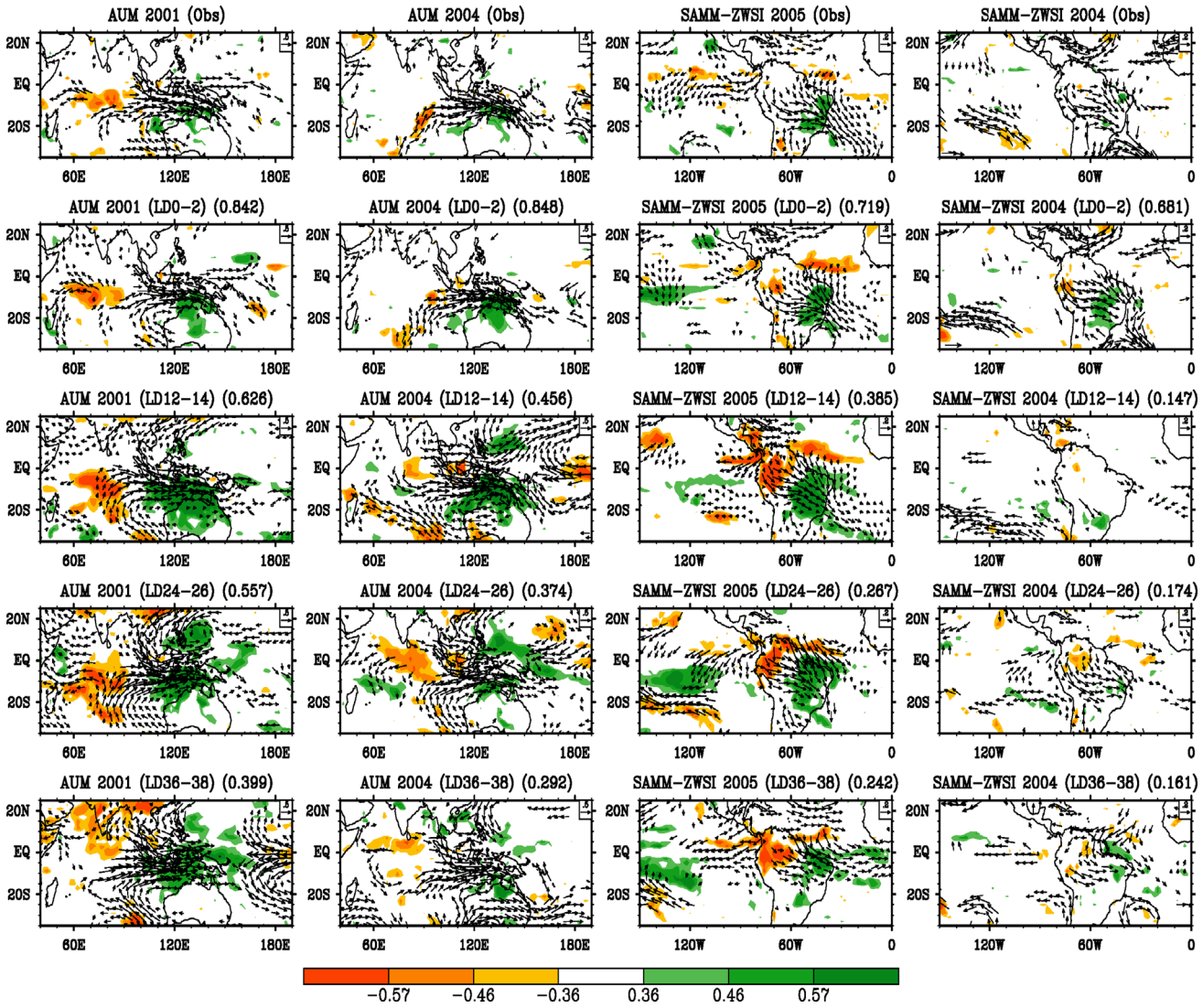

Fig. 10 Same as Fig. 9, but for the Australian monsoon index and the South American monsoon index

However, with increasing leads, the strong convection over northern Australia and the CEF across the Maritime Continent to the southern hemisphere seem to be more significantly related to the AUM index. Nevertheless, along with the strengthening link with tropical circulation in the southern and northern hemispheres, the variability of AUM is still excellently captured by the southeasterly wind over the west coast of Australia in 2001. In contrast, with advancing lead time, the strengthening connection of AUM to large-scale circulation quickly shields the observed regional link between AUM and the zonal wind over northern Australia in 2004.

As also shown by Fig. 10, the observed ZWSI for the SAMM is best correlated with northerly wind over the Amazon Basin and Brazil and with precipitation over southeastern Brazil. The forecast in 2005 tends to show an apparent response of larger-scale circulation to the convection over Brazil so that the relationship between the ZWSI and atmospheric circulation is reasonably well persistent at all-lead forecasts. For 2004, however, such a feature is not found and the forecasted ZWSI shows an excessively strong connection with regional circulation.

The relationships between NAMM/WAFM and circulation are presented in Fig. 11, in which monsoon indices are area-averaged precipitation shown in Fig. 7. Comparisons between 2000 and 2010 for NAMM precipitation and between 2005 and 2010 for WAFM precipitation indicate that the long-lead forecasts depict a link between NAMM precipitation and cyclonic wind anomaly over the northeastern Pacific and a link between WAFM precipitation and cyclonic wind anomaly from the equatorial eastern Atlantic to West Sahara, respectively. Therefore, forecasts may be more skillful when observed monsoon precipitation has such a similar connection with circulation over a

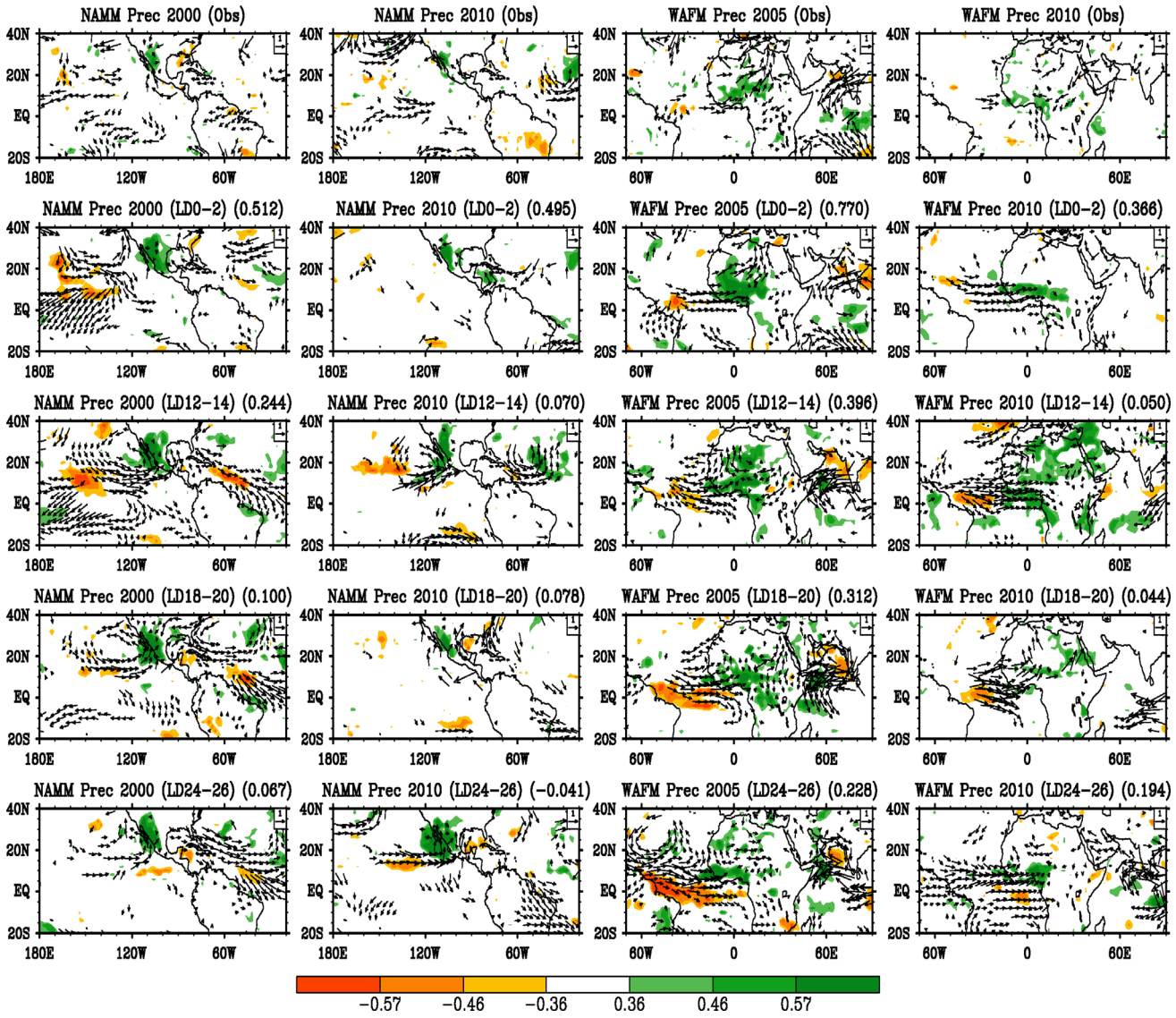

Fig. 11 Same as Fig. 9, but for the area-averaged precipitation over North America monsoon region (*left two columns*) and West African monsoon region (*right two columns*) instead of dynamical monsoon indices

relatively broad area than when precipitation is linked with regional circulation.

The above comparisons imply that the model tends to depict the response of large-scale atmospheric circulation to tropical convection with increasing lead time, and the prediction skill of a monsoon index may depend partially on the extent to which observed variability of the monsoon index is attributed to the variation of large-scale circulation. This feature can also be found from the comparisons of other cases, e.g., the forecasts in 2000 and 2010 for SEAM, 2002/2005 and 2010/2007 for SAM, 2005 and 2008 for AUM, and 2001 and 2004 for MWSI of SAMM (figures not shown).

5 Subseasonal variations of biases with monsoon evolution and lead time

We further discuss the subseasonal variations of biases as a function of prediction period and lead time. In addition to discussion of the variation features of biases for individual fields, multivariate empirical orthogonal function (EOF) analyses are carried out for the biases of 850-hPa winds, precipitation, and surface temperature over various monsoon regions. The predictions of all leads from zero to 40 days are involved in the EOF computations. For the sake of clarity, results for precipitation and surface temperature are discussed separately.

5.1 Asian summer monsoon

Pentad climatologies of precipitation and 850-hPa winds in different Julian pentads for ensemble predictions with leads of 0–2 days and 24–26 days show reasonable features of subseasonal evolution of the Asian summer monsoon. The differences between predictions and observations (Fig. 12) show the variations of biases with forecast period and lead time. These variations include the migrations of the cyclonic wind bias and associated precipitation bias over the northwestern Pacific and the change in biases over the tropical Indian Ocean from anticyclonic wind and insufficient rainfall in early May to cyclonic wind and excessive precipitation in July and August. They also include the persistence of dry bias over the northwestern Bay of Bengal during monsoon season and the reinforcement of biases of winds and precipitation over many places, especially the equatorial Indian Ocean, from short leads to long leads.

Figure 13a–c show the latitude-time cross sections for biases of surface temperature along 70°–100°E for ensemble-mean predictions of different leads. Almost in all predictions, apparent warm biases over the Tibetan Plateau (30°–40°N) persist in summer even though with a significant weakening from July. Among the latitude belt of 10°–30°N, a change from cold to warm biases occurs around mid-June at longer leads, while an opposite conversion from warm to cold biases appears around late June at shorter leads. Besides, the small biases to the south of 10°N at shorter leads are replaced by larger biases at longer leads, which are also featured by a warm-to-cold transition in June. Over the northwestern Pacific (Fig. 13d–f), a transition from cold bias to warm bias occurs over the subtropics near late June and early July, probably associated with the shift of the cyclonic wind bias over the western Pacific. Meanwhile, the warm biases over tropical areas persist in the entire boreal summer and often strengthen with increasing lead time.

The multivariate EOF analyses of the biases of 850-hPa winds, precipitation, and surface temperature of all leads are shown in Fig. 14. Similar to the features shown in Figs. 1, 2 and 3, the first mode (not shown, the same hereafter) indicates that the Asian monsoon is weaker than observed in most of summer. It is further revealed by Fig. 14c that the biases associated with this mode gradually intensify before formation of the strongest SAM and full control of the WPSH over the northwestern Pacific and weaken with the retreat of SAM and WPSH (see Figs. 13, 14 in Liu et al. 2012). The second mode features a transition of biases from anticyclonic wind to cyclonic wind across the Indian Peninsula and the equatorial Indian Ocean and from the northwesterly wind bias in the tropics and anticyclonic wind bias in the subtropics to an opposite-sign distribution over the northwestern Pacific, along with a consistent variation of biases in precipitation. The transition occurs around late June and early July, when the SAM reaches its peak and the WPSH is in a northward shifting process. Although the second mode has a smaller variance, its typical features can be captured by the predictions of individual fields (see description for Fig. 12) because the second mode is in a strong state when the first mode is in a weak state as depicted by Fig. 14c, d.

The result for winds and surface temperature (Fig. 14b) further indicates that the transition of biases of winds over the SAM region shown in the second mode is associated with a reversal of biases of surface temperature from the equatorial Indian Ocean across South Asia to the Tibetan Plateau (also see Fig. 13a–c). Considering the evolution features of the magnitude of SAM and the position of WPSH, the first mode represents the dominance and persistence of weaker-than-observed SAM and WPSH in boreal summer, and the second mode can be explained from the following two aspects. First, over the northwestern Pacific, the weaker WPSH before July can contribute to the cyclonic wind bias south of 20°N and the northwesterly wind bias near the equator. The northward shift of WPSH around July favors a northward movement of cyclonic wind bias that intensifies the southeasterly wind bias near the equator. Meanwhile, it is helpful for the biases of precipitation and surface temperature to be replaced by opposite-sign biases during the transition process. Secondly, the transition of biases of winds and precipitation over the SAM region is not only connected to the reversal of biases of surface temperature over the equatorial Indian Ocean and near India through heat flux transportation and upwelling processes, but also attributed partially to the change from warm bias to cold bias over the Tibetan Plateau, favoring the transition of zonal wind bias in the south as a thermal response of regional atmospheric circulation.

5.2 West African summer monsoon

Results of multivariate EOF analysis for WAFM are shown in Fig. 15. Also, the subseasonal variations of individual fields of winds, precipitation, and surface temperature are analyzed but the figures are not all shown (same hereafter in Sect. 5).

The underestimated precipitation over most of West Africa except the southwestern corner does not lead to warming of land surface at the south of 15°N in the first mode. Thus, the biases of winds and precipitation in the first mode may be attributed to the rapid occurrence of conspicuous warm bias over the Sahara Desert and cold bias over tropical West Africa, which maximize near 2 °C at the leads of about 1 week (Fig. 13g–i). Especially, the apparent warm bias over the Sahara has appeared at the minimum leads. This thermal bias distribution may induce a regional

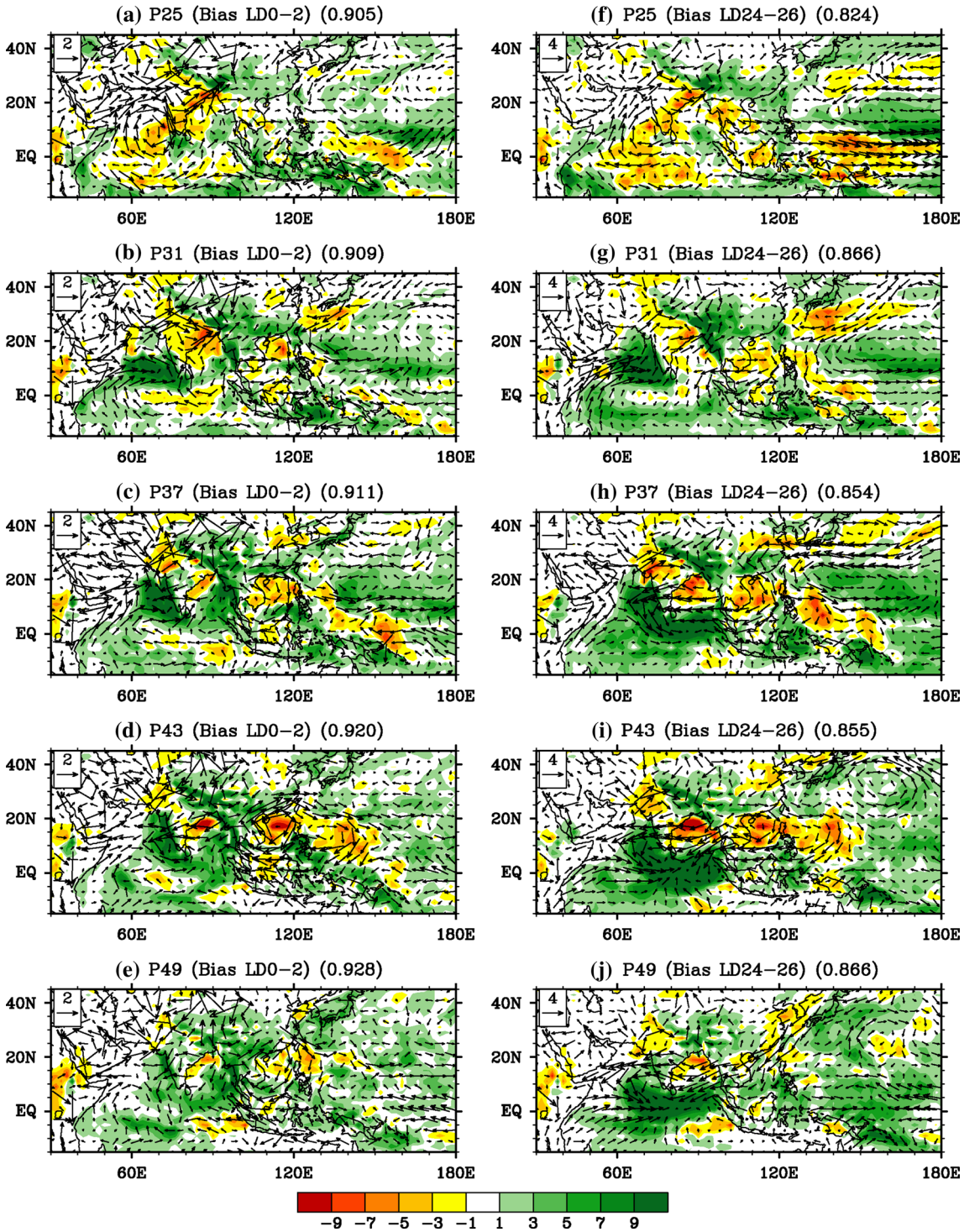

Fig. 12 Biases of climatological pentad precipitation (*shadings*, units mm/day) and 850-hPa winds (*vectors*, units ms^{-1}) for different Julian pentads in summer monsoon season for ensemble predictions with leads of 0–2 days (*left column*) and 24–26 days (*right column*). The *decimals* shown in right of headlines are spatial pattern correlations between predictions and observations

low-level circulation bias, which suppresses convergence and results in a dry bias over the WAFM region.

The second mode is characterized by a reversal of wind and precipitation biases near the Gulf of Guinea around July, which is likely related to the northward shift of ITCZ and the intensification of southerly CEF over the eastern equatorial Atlantic, leading to strengthening monsoon precipitation from July. The warm state over the Sahara attains its peak during this time and then begins a gradually weakening process, along with a

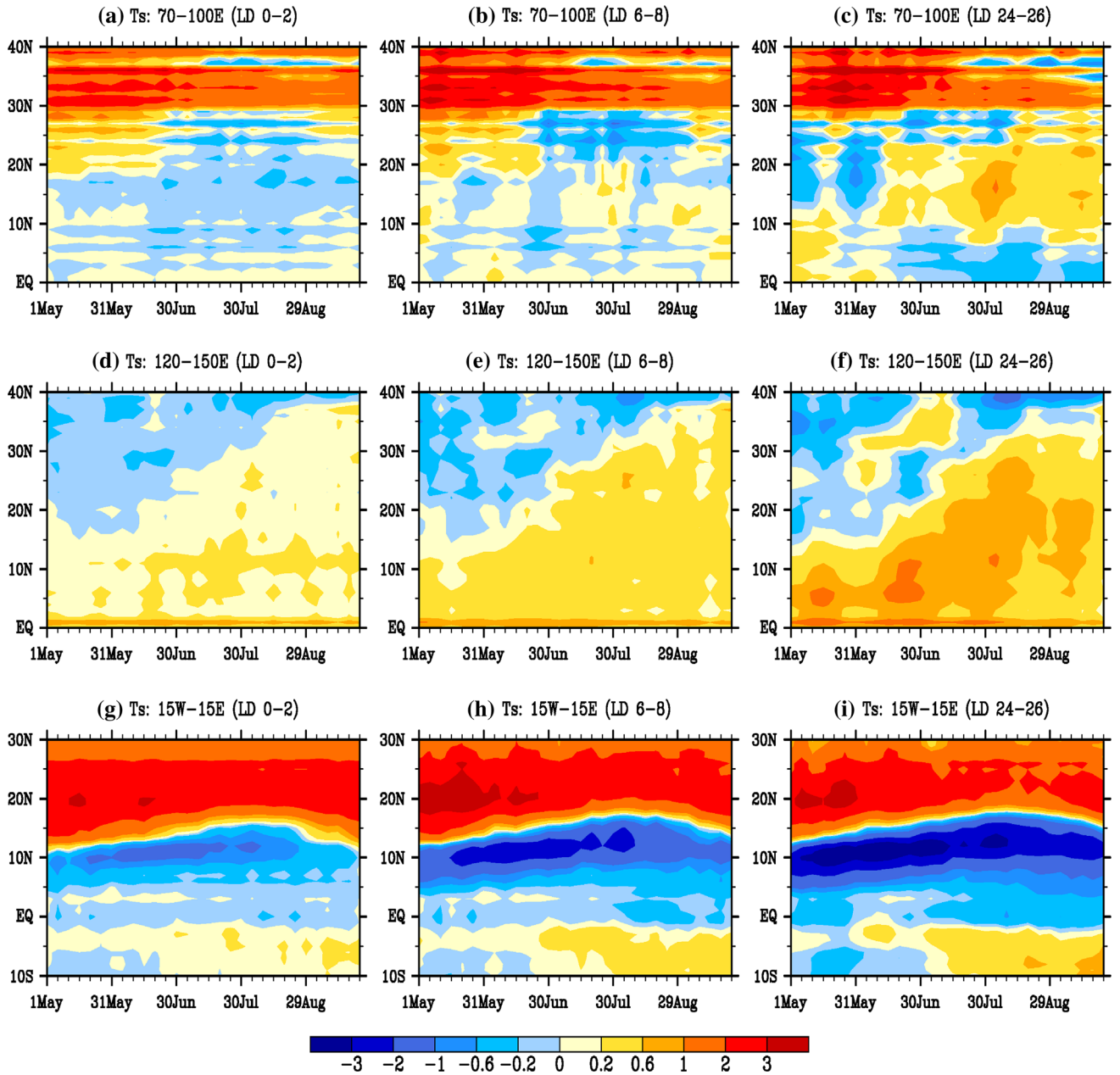

Fig. 13 Latitude-time cross sections of prediction biases of surface temperature (units °C) along 70°–100°E (*top row*), 120°–150°E (*middle row*), and 15°W–15°(*bottom row*) for ensemble-mean predictions of different leads

decrease in warm bias over the Sahara and weakening of cold bias in tropical West Africa. Particularly, associated with the northward shift of ITCZ and the boundary line between warm and cold biases, the surface temperature near 15°N shows a transition from warm bias to cold bias (Fig. 13g–i).

Therefore, it seems that the regional impacts of the strong warm bias over the Sahara and the cold bias over the tropical monsoon region play an important role in the formation of dry bias over West Africa. The northward shift of ITCZ and the change in underlying thermal state can weaken the dry bias to a certain degree in the latter part of summer monsoon season.

5.3 North American summer monsoon

Figure 16 shows the results of multivariate EOF analysis for NAMM. The first mode exhibits weaker-than-observed monsoon low and Bermuda High in the model. The second mode is characterized by transitions from anticyclonic wind bias to cyclonic wind bias over the extratropical northeastern Pacific and the northwestern Atlantic, and

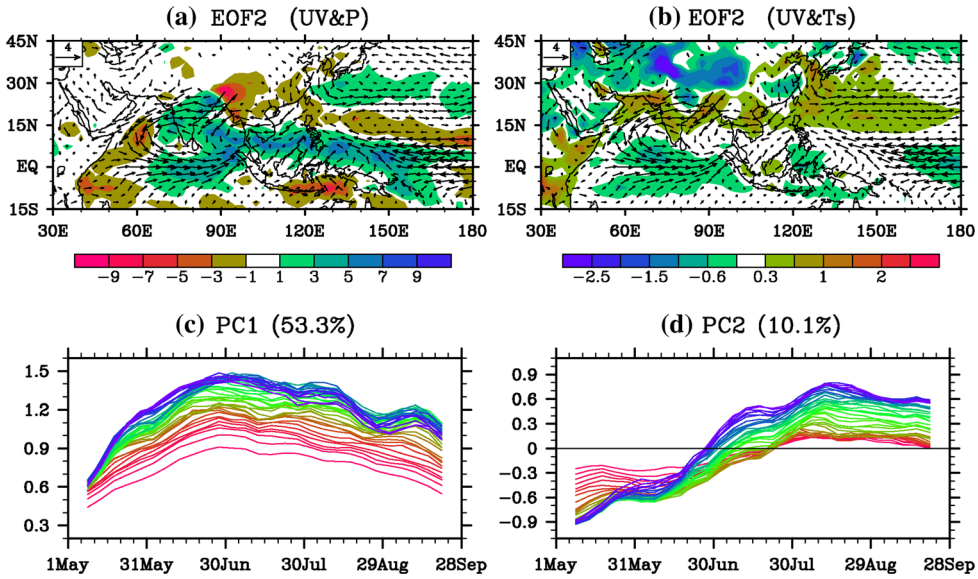

Fig. 14 Multivariate EOF analysis of the prediction biases of 850-hPa winds, precipitation, and surface temperature for all leads. With the same distribution of winds (*vectors* in **a** and **b**), features for precipitation (*shading* in **a**) and surface temperature (*shading* in **b**) in the second mode (first mode not shown) are given separately in the *top row*, and three-point running averaged principal components are shown in the *bottom row*. The color range from the *red* end to the *blue* end in (**c**) and (**d**) denotes the leads from 0 to 40 days

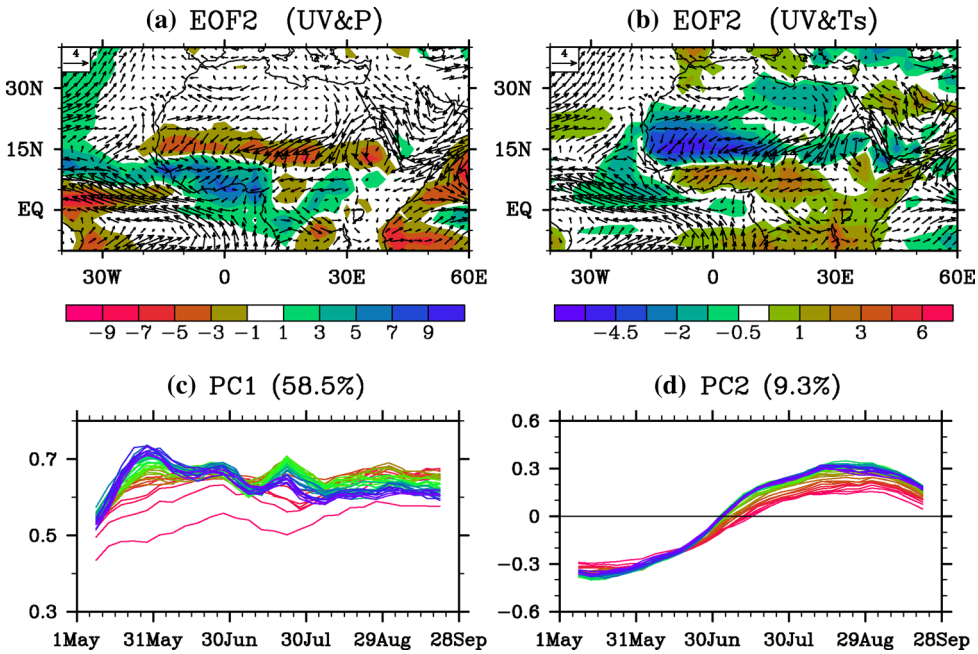

Fig. 15 Same as Fig. 14 but for the multivariate EOF analysis for the West African summer monsoon

from cyclonic wind bias to anticyclonic wind bias over the subtropical eastern Pacific and the southwest coast of North America. As a result, a change in precipitation from wet bias to dry bias occurs over the NAMM region around early July. The biases of regional circulation and precipitation over eastern-central North America, although weak, also exhibit transitional changes.

The apparent warm bias over the subtropical eastern Pacific captured by the first mode seems to be associated with the anticyclonic wind bias near the NAMM region, while the gradually intensifying cold bias over eastern-central North America may be linked to the strong anticyclonic wind bias and dry bias over the region thorough thermal response of regional circulation. The features depicted by the second mode mainly reflect the occurrence of transitions from anticyclonic wind bias to cyclonic wind bias for the Pacific High and the Bermuda High, and from cyclonic bias to anticyclonic bias for the monsoon low. In addition, as suggested by the two modes, the variations of wind and precipitation biases over eastern-central North America may be affected by regional or mid-high latitude factors.

5.4 Australian summer monsoon

Results of multivariate EOF analysis for AUM are analyzed. The first mode presents a stronger but more northward ITCZ and corresponding warmer sea water over

northern Australia in the model. Figure 17a and b show a transition of biases of winds, precipitation, and surface temperate in the second mode. Due to the southward movement of ITCZ from the northern hemisphere to the southern hemisphere, the CEF near the Maritime Continent shows a change from southerly flow to northerly flow, and the winds over the adjacent tropical regions also show opposite distributions between the early and late periods of monsoon (figure not shown). Along with the above process, there are transitions for winds from divergence bias to convergence bias and for precipitation from dry bias to wet bias to the north of Australia. Also, the dry bias over northern Australia, which persists in most of monsoon season, is weak in November and December and becomes strong in January and February. Correspondingly, the surface temperature over northern Australia shows a reversal change from cold bias to warm bias.

5.5 South American summer monsoon

Figure 18 shows the results of multivariate EOF analysis for SAMM. The first mode denotes that, in the SAMM region, the weak northerly CEF in the northern Amazon Basin and the overestimated precipitation near the Andes are often predicted by model. The subseasonal variations of individual fields (figure not shown) indicate that the weaker-than-observed CEF should play a crucial part in the formation of dry bias in northern South America, and the biases of subtropical highs in the Pacific and the Atlantic may partially account for the wind biases in the neighboring regions of South America. Nevertheless, the northerly wind bias from the southwestern Amazon Basin to the La Plata Basin may be partially related to the apparent cold bias from southeastern Brazil to northern Argentina.

The second mode is featured by a clear reversal of bias of winds in austral summer, indicating transitions of the subtropical highs over the Pacific and the Atlantic from weaker to stronger state near South America, as well as the change in northerly CEF from weaker to stronger state accompanied by a southward shift of the ITCZ. Correspondingly, the dry bias over most of South America is weakened or even regionally replaced by wet bias in late monsoon period (figure not shown). However, the biases of surface temperature do not show apparent development over most areas except near the equatorial eastern Pacific and the La Plata Basin.

5.6 Bias growth with lead time

The principal components also show that the time for biases to reach saturation state experiences significant geographical differences. As depicted by Figs. 14, 15, 16, 17, and 18c, the biases of associated winds, precipitation, and surface temperature over the Asian monsoon, SAMM, and AUM regions, especially the last one, show gradual growth with increasing lead time. It often takes nearly 1 month for them to reach the peaks. These features suggest a potentially large persistence of initial memory of the climate system and a probably high skill for these monsoon areas. However, over the regions for WAFM and NAMM, mostly the biases need only a few days to attain their peaks, possibly relating to the clear initial shock and quick skill loss of precipitation as previously shown in Fig. 4.

The principle components of various leads of the second mode often show much smaller differences compared to the first mode. That is, small spreads of biases at different leads are easily found even they vary with monsoon regions, variables, mode phases, and ranges of lead time. Particularly, the biases of second mode for Asian monsoon

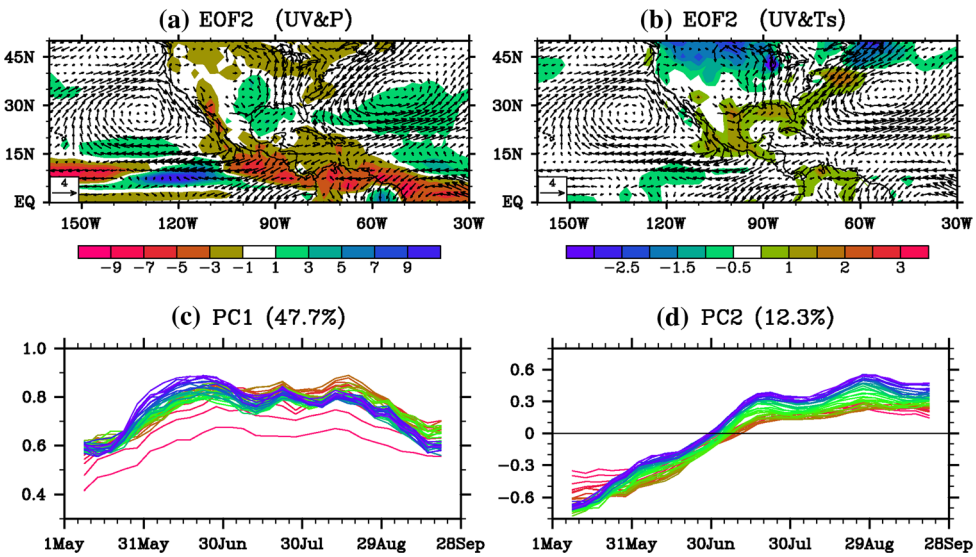

Fig. 16 Same as Fig. 14 but for the multivariate EOF analysis for the North American summer monsoon

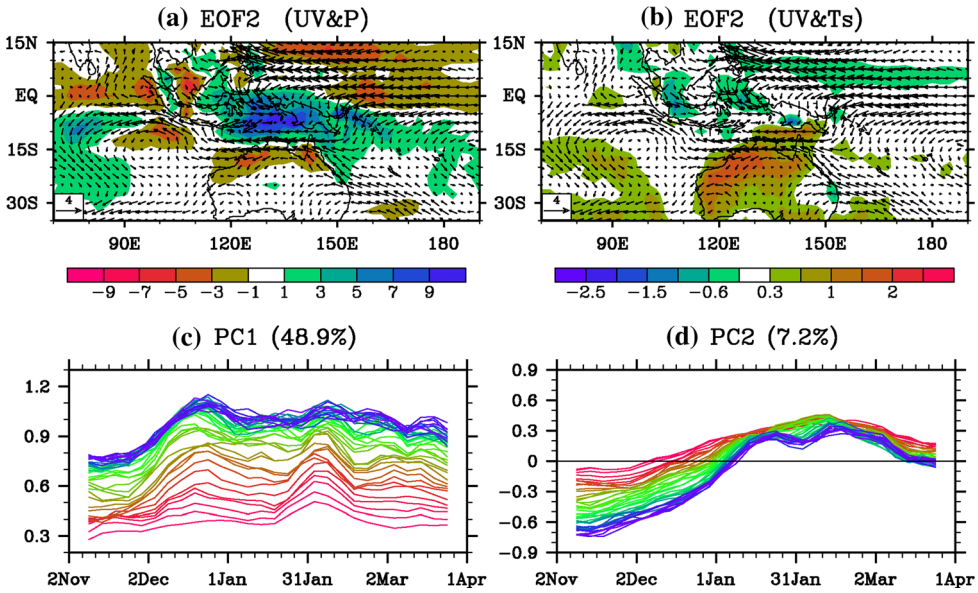

Fig. 17 Same as Fig. 14 but for the multivariate EOF analysis for the Australian summer monsoon

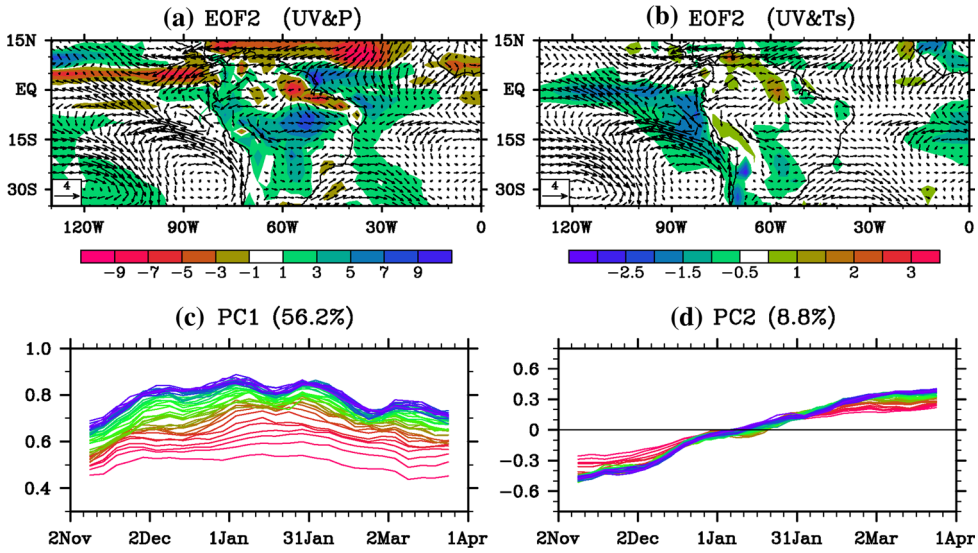

Fig. 18 Same as Fig. 14 but for the multivariate EOF analysis for the South American summer monsoon

exhibit fast growth within short leads before July and major development within long leads after July (Fig. 14d), which suggests that slowly varying components of the coupled system begin to exert a gradually important influence on the biases after the transition process. Also, the biases of second mode for AUM show a very slow increase with lead time before the transition process in contrast to an immediate growth and saturation afterwards (Fig. 17d).

6 Conclusion and discussion

In this study, we have diagnosed the subseasonal forecast skills and prediction biases of global summer monsoons using retrospective forecasts by the NCEP CFSv2. The prediction skills of subseasonal monsoon variability are evaluated by RMSE and correlations of zonal wind and precipitation between the CFSv2 and observations. The error growth of zonal wind is mainly concentrated in the leads <2 weeks over most regions, except over southern Asia in boreal summer and tropical northern Australia in austral summer where a longer duration of error development implies more actual predictability. The error growth of precipitation is mostly concentrated within the leads of about 1 week, and the prediction suffers by initial shocks over some regions, especially over subtropical Asia and the tropical areas from the eastern Pacific to West Africa in boreal summer. Zonal wind also exhibits better correlation skill over the Asian-Australian tropical monsoon regions than other regions, while precipitation presents a very quick decrease in prediction skill with increasing leads. Nevertheless, the area-averaged precipitation over certain

monsoon regions is sometimes predicted with high skill, although with an apparent interannual difference.

The lead time for most dynamical monsoon indices to become unpredictable is about 2–3 weeks on average, but it shows apparent interannual differences featured by contrast between up to 5 weeks in some years and <2 weeks in other years. Especially, the predictions for Asian and Australian monsoon indices sometimes maintain a nearly unchanged skill or a gradually increasing skill that is above the significance level at leads longer than 2–3 weeks. For some indices, comparisons of their relationships with atmospheric circulation and precipitation between skillful and unskillful cases are further conducted. The forecast skills for certain indices depend partially on the extent to which observed variability of the indices is attributed to the variation of large-scale circulation. Thus, the predictions of the subseasonal variability of a monsoon index tend to be more (less) skillful when the index is closely linked to atmospheric circulation over a larger (smaller) spatial range.

The variation of biases with prediction period and lead time are also explored by analyses of subseasonal variations of individual fields and multivariate EOF analyses of winds, precipitation, and surface temperature. The first and second modes for various monsoons are featured by persistently existing biases and transitional biases, respectively. Weaker-than-observed SAM, SEAM, WAFM, and NAMM in boreal summer and underestimated AUM and SAMM in austral summer are often captured by the model. However, these features are regionally and temporally offset or intensified by the secondary but important transitional processes of biases, which are partially related to the northward shift of WPSH, the reversal of surface temperature biases over the SAM and WAFM regions, the migration of ITCZ, and the transitions of subtropical highs near the NAMM and SAMM regions. For the primary modes, bias growth with increasing leads is much slower over the Asian monsoon, SAMM, and AUM regions than over the WAFM and NAMM regions, implying potentially longer persistence of initial memory of the climate system for the former than for the latter. In addition, the spreads of biases at various leads shown in the second modes exhibit apparent variations with the phase of the modes and the range of lead time, suggesting different contributions from slow-varying and fast-varying components of the climate system.

The subseasonal forecast skills of monsoons and their interannual differences are preliminarily explored but the source of forecast skills is not addressed in this study. It should be noted that the variations of SEAM index are more predictable by the model for 1999, 2000, and 2008 than for 2005 and 2010 due partially to its closer link with larger-scale circulation and convection for the former than for the latter (see discussion of Figs. 7b, 9). To a certain extent, this feature implies that the forecasts for subseasonal variability of SEAM tend to be more skillful in the summer following La Niña than El Niño, possibly attributed to the apparently enhanced and suppressed convections near the Philippines in the decaying stage of La Niña and El Niño, respectively (Xie et al. 2009). However, the skills for most monsoon indices are found to show insignificant correlation with ENSO. This feature suggests that although the ENSO does not necessarily linearly affect monsoon variation, it sometimes may act as an important background to modulate the skills of forecast. Nevertheless, this conclusion needs to be investigated further for two aspects. (a) The effects of interannually varying external forcing are often represented as seasonally persistent anomalies (Krishnamurthy and Shukla 2007; Achuthavarier and Krishnamurtky 2010), which affect the time-mean values of pentad anomaly sequences but do not influence the results of forecast skills because the temporal correlation between two sequences does not depend on their respective sequence means. Or equivalently, it can also be assumed that the interannual variability introduced by external forcing is removed when the seasonal averages of pentad anomalies are subtracted during the computation of temporal correlation. (b) The data length in this study is not long enough for exploring the relationship of subseasonal forecast skills with ENSO. Thus, more experiments and further analyses are needed for understanding above results.

It should also be realized that our results are based on the hindcasts by the NCEP CFSv2. The prediction skills and biases of monsoon, however, are often model dependent. Apparent model-to-model differences of prediction biases and skills have been found by previous studies (e.g., Wang et al. 2008; Lee et al. 2010; Xue et al. 2010; Li et al. 2012; Rajeevan et al. 2012). Thus, further evaluations on monsoon subseasonal predictions by different state-of-the-art climate models are necessary for better understanding monsoon predictability and multi-model ensemble predictions.

Acknowledgments The authors thank two anonymous reviewers for their fruitful suggestions, which are helpful for improving the overall quality of the manuscript. This study was partially supported by the National Basic Research Program of China (973 Program: 2010CB951903), the National Natural Science Foundation of China (Grants 41275076, 41105061 and 40905046), Sun Yat-sen University "985 Project" Phase 3, and the NOAA—China Meteorological Administration Bilateral Program.

References

Achuthavarier D, Krishnamurtky V (2010) Relation between intraseasonal and interannual variability of the South Asian monsoon

in the National Centers for Environmental Predictions forecast systems. J Geophys Res 115:D08104. doi:10.1029/2009JD012865
Charney JG, Shukla J (1981) Predictability of monsoons. In: Lighthill J, Pearce RP (eds) Monsoon dynamics. Cambridge University Press, Cambridge, pp 99–109
Chen D, Cane MA, Zebiak SE, Cañizares R, Kaplan A (2000) Bias correction of an ocean–atmosphere coupled model. Geophys Res Lett 27:2585–2588. doi:10.1029/1999GL011078
Drbohlav HKL, Krishnamurthy V (2010) Spatial structure, forecast errors, and predictability of the South Asian monsoon in CFS monthly retrospective forecasts. J Clim 23:4750–4769
Fu X, Wang B, Bao Q, Liu P, Lee J (2009) Impacts of initial conditions on monsoon intraseasonal forecasting. Geophys Res Lett 36:L08801. doi:10.1029/2009GL037166
Gan MA, Rao VB, Moscati MCL (2005) South American monsoon indices. Atmos Sci Lett 6:219–223
Goswami BN, Krishnamurthy V, Annamalai H (1999) A broad-scale circulation index for the interannual variability of the Indian summer monsoon. Q J R Meteorol Soc 125:611–633
Higgins W, Silva VBS, Kousky VE, Shi W (2008) Comparison of daily precipitation statistics for the United States in observations and in the NCEP Climate Forecast System. J Clim 21:5993–6014
Jones C, Carvalho LMV, Liebmann B (2012) Forecast skill of the South American monsoon system. J Clim 25:1883–1889
Joyce RJ, Janowiak JE, Arkin PA, Xie P (2004) CMORPH: A method that produces global precipitation estimates from passive microwave and infrared data at high spatial and temporal resolution. J Hydromet 5:487–503
Kajikawa Y, Wang B, Yang J (2009) A multi-time scale Australian monsoon index. Int J Clim 30:1114–1120
Kang IS et al (2002) Intercomparison of the climatological variations of Asian summer monsoon precipitation simulated by 10 GCMs. Clim Dyn 19:383–395
Krishnamurthy V, Shukla J (2007) Intraseasonal and seasonally persisting patterns of Indian monsoon rainfall. J Clim 20:3–20
Krishnamurti TN, Mitra AK, Kumar TS, Yun WT, Dewar WK (2006) Seasonal climate forecasts of the South Asian monsoon using multiple coupled models. Tellus A 58:487–507
Kumar KK, Hoerling M, Rajagopalan B (2005) Advancing dynamical prediction of Indian monsoon rainfall. Geophys Res Lett 32:L08704. doi:10.1029/2004GL021979
Lau KM, Kim KM, Yang S (2000) Dynamical and boundary forcing characteristics of regional components of the Asian summer monsoon. J Clim 13:2461–2482
Lee JY et al (2010) How are seasonal prediction skills related to models' performance on mean state and annual cycle? Clim Dyn 35:267–283
Lee SS, Lee JY, Ha KJ, Wang B, Schemm JKE (2011) Deficiencies and possibilities for long-lead coupled climate prediction of the Western North Pacific–East Asian summer monsoon. Clim Dyn 36:1173–1188
Li Y, Yang S (2010) A dynamical index for the East Asian winter monsoon. J Clim 23:4255–4262
Li C, Lu R, Dong B (2012) Predictability of the western North Pacific summer climate demonstrated by the coupled models of ENSEMBLES. Clim Dyn 39:329–346
Liang J, Yang S, Hu Z, Huang B, Kumar A, Zhang Z (2009) Predictable patterns of Asian and Indo-Pacific summer precipitation in the NCEP CFS. Clim Dyn 32:989–1001
Liu X, Yang S, Kumar A, Weaver S, Jiang X (2012) Diagnostics of subseasonal prediction biases of the Asian summer monsoon by the NCEP Climate Forecast System. Clim Dyn. doi:10.1007/s00382-012-1553-3
Misra V (2008) Coupled interactions of the monsoons. Geophys Res Lett 35:L12705. doi:10.1029/2008GL033562
Misra V, Zhang Y (2007) The fidelity of NCEP CFS seasonal hindcasts over Nordeste. Mon Wea Rev 135:618–627
Moron V, Philippon N, Fontaine B (2004) Simulation of West African monsoon circulation in four atmospheric general circulation models forced by prescribed sea surface temperature. J Geophys Res 109:D24105. doi:10.1029/2004JD004760
Pegion K, Sardeshmukh PD (2011) Prospects for improving subseasonal predictions. Mon Wea Rev 139:3648–3666
Pope VD, Stratton RA (2002) The processes governing horizontal resolution sensitivity in a climate model. Clim Dyn 19:211–236
Rajeevan M, Unnikrishnan CK, Preethi B (2012) Evaluation of the ENSEMBLES multi-model seasonal forecasts of Indian summer monsoon variability. Clim Dyn 38:2257–2274
Saha S et al (2006) The NCEP Climate Forecast System. J Clim 19:3483–3517
Saha S et al (2010) The NCEP Climate Forecast System Reanalysis. Bull Am Meteor Soc 91:1015–1057
Turner AG, Inness PM, Slingo JM (2005) The role of the basic state in the ENSO–monsoon relationship and implications for predictability. Q J R Meteorol Soc 131:781–804
Vera C et al (2006) Toward a unified view of the American monsoon systems. J Clim 19:4977–5000
Wang B, Fan Z (1999) Choice of South Asian summer monsoon indices. Bull Am Meteor Soc 80:629–638
Wang B, Kang IS, Lee JY (2004) Ensemble simulations of Asian–Australian monsoon variability by 11 AGCMs. J Clim 17:803–818
Wang B, Ding QH, Fu XH, Kang IS, Jin K, Shukla J, Doblas-Reyes F (2005) Fundamental challenge in simulation and prediction of summer monsoon rainfall. Geophys Res Lett 32:L15711. doi:10.1029/2005GL022734
Wang B et al (2008) How accurately do coupled climate models predict the leading modes of Asian–Australian monsoon interannual variability? Clim Dyn 30:605–619
Weaver SJ, Wang W, Chen M, Kumar A (2011) Representation of MJO variability in the NCEP Climate Forecast System. J Clim 24:4676–4694
Webster PJ, Yang S (1992) Monsoon and ENSO: selectively interactive systems. Q J R Meteorol Soc 118:877–926
Wen M, Yang S, Vintzileos A, Higgins W, Zhang R (2012) Impacts of model resolutions and initial conditions on predictions of the Asian summer monsoon by the NCEP Climate Forecast System. Wea Forecasting 27:629–646
Xie SP, Hu K, Hafner J, Tokinaga H, Du Y, Huang G, Sampe T (2009) Indian Ocean capacitor effect on Indo-western Pacific climate during the summer following El Niño. J Clim 22:730–747
Xue Y et al (2010) Intercomparison and analyses of the climatology of the West African monsoon in the West African monsoon modeling and evaluation project (WAMME) first model intercomparison experiment. Clim Dyn 35(1):3–27
Yhang YB, Hong SY (2008) Improved physical processes in a regional climate model and their impact on the simulated summer monsoon circulations over East Asia. J Clim 21:963–979
Yang S, Zhang Z, Kousky VE, Higgins RW, Yoo SH, Liang J, Fan Y (2008a) Simulations and seasonal prediction of the Asian summer monsoon in the NCEP Climate Forecast System. J Clim 21:3755–3775
Yang S, Wen M, Higgins RW (2008b) Sub-seasonal features of the Asian summer monsoon in the NCEP Climate Forecast System. ACTA Oceanologica Sinica 27:88–103
Yang S, Jiang Y, Zheng D, Higgins W, Zhang Q, Kousky VE, Wen M (2009) Variations of U.S. regional precipitation and simulations by the NCEP CFS: focus on the southwest. J Clim 22:3211–3231
Yang S, Wen M, Yang R, Higgins W, Zhang R (2011) Impacts of land process on the onset and evolution of Asian summer

monsoon in the NCEP Climate Forecast System. Adv Atmos Sci 28:1301–1317

Yuan X, Wood EF, Luo L, Pan M (2011) A first look at Climate Forecast System version 2 (CFSv2) for hydrological seasonal prediction. Geophys Res Lett 38:L13402. doi:10.1029/2011GL047792

Zhou T, Wu B, Wang B (2009) How well do atmospheric general circulation models capture the leading modes of the interannual variability of the Asian–Australian monsoon? J Clim 22: 1159–1173